Special Collection

Interaction between Electrolytes and Sb_2O_3-Based Electrodes in Sodium Batteries: Uncovering the Detrimental Effects of Diglyme

Kristina Pfeifer,[a] Miryam Fayena Greenstein,[b] Doron Aurbach,[b] Xianlin Luo,[a] Helmut Ehrenberg,[a, c] and Sonia Dsoke*[a, c]

Conversion materials are promising to improve the energy density of sodium-ion-batteries (NIB). Nevertheless, they suffer from the drawback of phase transitions and pronounced volume changes during cycling, which causes cell instability. When using these types of electrodes, all cell-components have to be adjusted. In this study, a tremendous influence of the electrolyte solution on Sb_2O_3 conversion electrodes for NIBs is discussed. Solutions based on three solvents and solvent combinations established for NIBs, ethylene carbonate/dimethyl carbonate (EC/DMC), EC/DMC + 5% fluoroethylene carbonate (FEC), and diglyme, lead to a massively divergent electrochemical behavior of the same Sb_2O_3 electrode. Sb_2O_3 demonstrates the highest stability in solutions containing FEC, because this component forms a flexible, protecting surface film that prevent disintegration. One key finding of this work is that electrolyte solutions based on ether solvents like diglyme can remove Sb-ions from Sb_2O_3 during cycling. Diglyme has the ability to coordinate and extract Sb^{3+} during the oxidation of Sb_2O_3. This leads to contaminations of all cell components and a strong capacity loss together with an irregular electrochemical signature. Due to its poor reactivity at low potentials, diglyme forms a thin or even no surface layer. Thereby, there are no protecting films on the Sb_2O_3 electrodes that can avoid Sb^{3+} ion dissolution. A critical examination of the electrolyte solutions components' impact is essential to match them with conversion reaction anodes.

1. Introduction

Energy storage technologies beyond lithium are of high interest since the demand for energy storage systems highly increased throughout the past years.[1] Lithium sources are exploited gradually. Thus, the price of this metal and its compounds is rising due to the growing electrification.[2] Sodium is one of the earth's most abundant elements. Therefore, NIBs are a promising alternative combining low cost and similar electrochemical behavior to that of LIBs.[3–6] Tremendous efforts have been made to develop suitable materials for NIB electrodes.[1,3,7] So far, a wide range of cathode materials have been discovered and explored in recent years. There are several types of cathode materials that can be considered as practical.[1,3,8] In turn, the anode side is a major challenge. It is important to develop high capacity/high durability negative electrodes for NIBs to promote their commercial development. Graphite, which is considered a commercial anode for lithium-ion batteries, cannot be used as an anode in sodium batteries, since energy constraint prevents sodium-ions from intercalation between the graphene layers. Other intercalation materials like $Na_2Ti_3O_7$[6] or $Li_4Ti_5O_{12}$[9,10] are well known for their high reversibility as the structural integrity is predominantly kept during sodiation and de-sodiation.[1,11] Still, a huge drawback is the low capacity originating from the intercalation mechanism.[8] Therefore, conversion type materials are described as prominent alternatives in the state-of-the-art literature.[8,12] The general operation formula for anodes working through conversion reactions is: $M_xX_y + zNa^+ + ze^- \rightleftharpoons xM^0 + yNa_{(z/y)}X$, where M is a metallic element and X the anion, for example, elements like oxygen, fluorine, nitrogen, sulfur and even phosphorous.[13] In order to ensure effective reactions with high specific capacity/rates, the M_xX_y reagents should be in the form of nano-particles. A full reduction of the active mass in the course of conversion reactions during discharge generally leads to higher specific capacities compared to intercalation compounds.[12,14] During charging, several compounds and phases may be formed, which can lead to complex electrochemical reactions. Additionally, phase transitions can be partially irreversible and even if they are fully reversible, they may involve pronounced volume changes in each cycle, which leads to morphological instability, including massive detrimental electrode cracking.[12,15,16] Hu *et al.*[17] reported promising features of Sb_2O_3 as anode material for NIBs. High specific

[a] K. Pfeifer, X. Luo, H. Ehrenberg, S. Dsoke
Institute for Applied Materials (IAM)
Karlsruhe Institute of Technology (KIT)
Hermann-von-Helmholtz-Platz 1, 76344 Eggenstein-Leopoldshafen, Germany
E-mail: sonia.dsoke@kit.edu
[b] M. F. Greenstein, D. Aurbach
Chemistry Department
Bar Ilan Institute for Nanotechnology and Advanced Materials
Bar-Ilan University
Ramat-Gan 5290002, Israel
[c] H. Ehrenberg, S. Dsoke
Helmholtz-Institute Ulm for Electrochemical Energy Storage (HIU)
P.O. Box 3640, 76021 Karlsruhe, Germany

Special Collection An invited contribution to a Special Collection dedicated to GDCh Electrochemistry: At the Interface between Chemistry and Physics

capacity, together with an exceptionally high rate performance and long cycling stability, were obtained due to the conversion-alloy mechanism, which was clarified in their work. These experiments were performed with alkyl carbonate-based electrolyte solutions, which are the most commonly used electrolyte solutions applied for both lithium and sodium-ion batteries.[1,4,8] Nevertheless, a study of Li *et al.*[18] reveals that different anode materials, for example, anatase TiO_2 or Sn, show superior Na^+ storage performance in ether-based electrolyte solutions like bis(2-methoxyethyl) ether (diglyme) when compared to alkyl carbonate-based solutions. The authors demonstrate that diglyme can facilitate sodiation-induced structural transitions of the TiO_2 and Sn. Furthermore, it enhances the charge transfer across the electrolyte solution/electrode interface due to the relatively low reactivity of diglyme towards alkali metals (Li, Na).[17] Additionally, Liu *et al.*[19] reported that the use of the glyme-based electrolyte stabilizes sodium metal and leads to low polarization of Na. Therefore, diglyme is considered as a promising alternative to alkyl carbonate-based electrolyte solutions in the state-of-the-art literature.[18–20]

On the contrary to the results of Li *et al.*[18], Brehm *et al.*[21] found that antimony shows very poor stability in the diglyme-based electrolyte solutions when compared to other studies where alkyl carbonate-based electrolyte solutions were used.[16,22,23] The reason was not further evaluated, offering a basis for this work. There are conflicting opinions on whether diglyme brings advantages or not. Especially the high concern of diglyme as reproductive toxin is an issue which always has to be considered. In this work, we choose Sb_2O_3, as an exemplary conversion reaction anode material for NIBs in order to investigate the relationships of electrolyte solutions with such an active material. The underlying mechanism is based on several phase transitions, which offers a complex system for the evaluation of the interaction between electrolyte solutions and this active material. We compare the electrochemical behavior of Sb_2O_3 in cells containing diglyme and alkyl carbonate-based electrolyte solutions and apply fundamental analytical tools for studying the electrodes and solutions after cycling. Our work provides an explanation for the poor behavior of Sb_2O_3 electrodes in diglyme containing NIBs and gives insights into the interaction of electrolytes with Sb based electrodes.

2. Results and Discussion

2.1. Sb_2O_3 Characterization

Figure 1a shows the refined X-ray diffraction pattern. All reflexes of the XRD pattern can be assigned to cubic Sb_2O_3 with the space group of $Fd\bar{3}m$ (ICSD: 240206). The obtained Rietveld parameters are: $a = b = c = 11.1571(1)$; R_p: 8.50; R_{wp}: 8.79. Scanning electron micrographs (Figure 1b) reveal that the commercial nanopowder consists of angular as well as spherical particles with a size of 50 nm–1 µm.

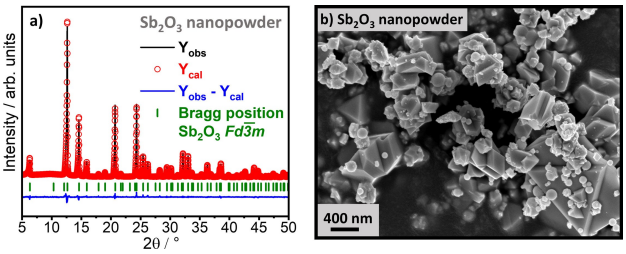

Figure 1. a) Rietveld-refined diffractogram, including the peak positions and b) scanning electron microscopy image of Sb_2O_3 powder.

2.2. Influence of the Electrolyte Solution on the Electrochemical Performance

The influence of the different electrolyte solutions on the electrochemical stability is demonstrated in Figure 2a and the corresponding Coulombic efficiency in Figure 2b. In order to simplify the discussion, the electrolyte solutions will be referred to as D (1 M $NaClO_4$ in diglyme), E (1 M $NaClO_4$ in EC/DMC) and F (1 M $NaClO_4$ in EC/DMC + 5 % FEC). Applying E as an electrolyte solution, the capacity drastically declines from 375 mAh g^{-1} to 75 mAh g^{-1} after 50 cycles. The capacity fading is accompanied by a decrease of the Coulombic efficiency from 97 % to 87 %, indicating an increase of irreversible side reactions. Such behavior is in line with our previous results revealing that sodium metal, which was used as counter and reference electrode, reacts with carbonate-based electrolyte solutions irreversibly forming problematic byproducts.[10] As a consequence, fast degradation appears in sodium metal-containing three-electrodes setups.[10]

A remarkable improvement is observed when FEC is added to the electrolyte solution. This can be attributed to superior solid electrolyte interphase (SEI) properties of both the working and the counter electrode.[24,25] When FEC is added to

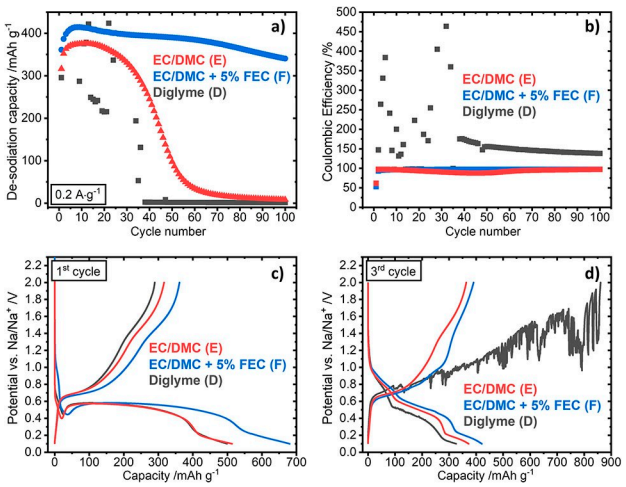

Figure 2. Sb_2O_3-based electrode cycled at 0.2 A g^{-1} in D, E and F solutions. a) Electrochemical cycling stability, b) coulombic efficiency, c) galvanostatic charge/discharge profiles of the 1st cycle, d) galvanostatic charge/discharge profiles of the 3rd cycle.

carbonate-based electrolyte solutions its reduction takes place on Li, Na and all kinds of reducing Li and Na compounds (including lithiated and sodiated products of conversion reactions). As a consequence, protective SEI layers that contain polymeric species and ionic Li or Na compounds are formed.[23,24,26–28] Such effects substantially contribute to the stability of the electrolyte solution, which contains FEC towards the sodium electrodes, as was shown in a previous work.[16] Additionally, the Coulombic efficiency stabilizes at 98% after 10 cycles, confirming a stabilization of the electrodes towards side reactions. Nevertheless, the processes are not entirely reversible, since, for rechargeable batteries, a Coulombic efficiency around 100% for both anode and cathode in the cells is mandatory.

Different from the behavior in the alkyl carbonates based solutions, an irregular capacity progress occurs for the ether-based electrolyte solution. Irregular de-sodiation capacity values between 50 $mAh\,g^{-1}$ and 420 $mAh\,g^{-1}$ are paired with a Coulombic efficiency $>100\%$ during the initial 35 cycles. Thereafter, the cell lost its entire capacity.

For a more detailed examination of this peculiar behavior, galvanostatic sodiation/de-sodiation voltage profiles of the first (Figure 2c) and third (Figure 2d) cycles are illustrated. The processes occurring during sodiation and de-sodiation was described by Hu *et al.*[17] as follows [Eqs. (1)–(7)]:

$$1.\ \text{sodiation}:\ Sb_2O_3\ (\text{cubic}) + xNa^+ + xe^- \rightarrow Na_xSb_2O_3 \quad (1)$$

$$Na_xSb_2O_3 + (6\text{-}x)e^- + (6\text{-}x)Na^+ \rightarrow 2Sb + 3Na_2O \quad (2)$$

$$1.\ \text{de-sodiation}:\ 2Sb + 3Na_2O \rightarrow Sb_2O_3\ (\text{amorphous}) + 6Na^+ + 6e^- \quad (3)$$

$$\text{Further sodiation}:\ Sb_2O_3\ (\text{amorphous}) + 6Na^+ + 6e^- \rightarrow 2Sb + 3Na_2O \quad (4)$$

$$2Sb + 2Na^+ + 2e^- \rightarrow 2NaSb \quad (5)$$

$$\text{Further de-sodiation}:\ 2NaSb \rightarrow 2Sb + 2Na^+ + 2e^- \quad (6)$$

$$2Sb + 3Na_2O \rightarrow Sb_2O_3\ (\text{amorphous}) + 6Na^+ + 6e^- \quad (7)$$

The first sodiation step is associated with a pronounced plateau at ~0.55 V, similar for all electrolytes. As described in equation (1) and (2), an intermediate compound $Na_xSb_2O_3$ is formed and further reduced to Sb and Na_2O. $Na_xSb_2O_3$ is solely present during the first sodiation. The higher capacity of the FEC-containing cell is, most probably, caused by the formation of a polymeric SEI.[23,26,28] Another plateau at about 0.1 V can be attributed to further sodiation of Sb (reaction (5)). Two processes can be determined at ~0.7 V and ~1.4 V during subsequent de-sodiation (Figure 2c), which are caused by the reactions described in equation (3) and (6). The galvanostatic profiles of Sb_2O_3 in alkyl carbonate-based electrolyte solutions do not change when comparing the first and third cycles (Figure 2c and d) following equations (4)–(7). Different from that, the galvanostatic de-sodiation profile of the cells cycled with electrolyte solution denoted as D demonstrates a severely irregular course starting from the second cycle. The irreversible capacity loss in the first cycle for solutions E, F and D is 38%, 47% and 42%, respectively. Such high capacity losses can be attributed to the partly irreversible phase transformations in the first cycle, as well as to the formation of the SEI. As previously described, a polymeric SEI is formed in the case of solution F. Such polymerization reactions can cause a higher initial capacity loss when compared to solution E.

To further understand the described phenomena, we performed an ex-situ characterization of the counter and working electrodes and the electrolyte solution after the process.

2.3. Ex Situ Characterization of Sb_2O_3 Electrodes

Scanning electron micrographs of the pristine electrode and the electrodes cycled 50 times in the respective electrolyte solutions are presented in Figure 3a-d. The pristine electrode (Figure 3a) consists of a well-distributed network of Sb_2O_3 particles with irregular polyhedral shape and C65 conductive additive. Massive differences are observed when comparing the pristine electrode with the electrodes cycled in alkyl carbonate-based solutions (Figure 3b, d). In the case of the electrolyte solution E (Figure 3b), a pronounced cracking of the electrode is observed. Additionally, a surface layer covers the entire electrode. Since no Sb_2O_3 particles are visible, most probably, the thick layer observed on the electrode surface after being cycled in solution E originates from decomposition products formed by side reactions between sodium and the electrolyte solution.[10] If the surface layer is not flexible enough, it should crack due to volume expansion during the conversion reaction, which in turn leads to new side reactions on the exposed parts of the electrode.[16] This matches to the poor performance of the cell cycled in electrolyte solution E (Figure 2a) and to the results obtained in our previous work.[10] The electrode cycled in solution F (Figure 3d) is also covered by a surface layer.

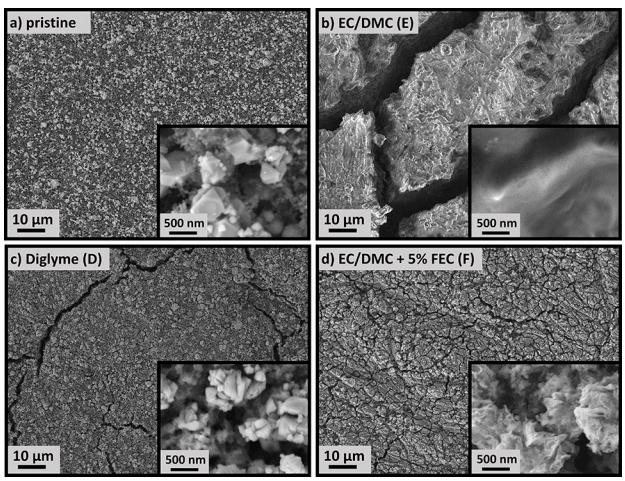

Figure 3. Scanning electron microscopy images with high magnification insets of Sb_2O_3 electrodes: a) pristine, b) after 50 cycles in solution E, c) after 50 cycles in solution D, d) after 50 cycles in solution F.

However, the electrode microstructure is still visible, indicating that the layer formed in electrolyte solution F is thinner than that formed in electrolyte solution E (Figure 3b). Furthermore, electrode's cracking is less distinct, most likely as a result of the flexible polymeric nature of the surface layers formed by reduction of FEC.[26,29] Considering the electrode, which was cycled in electrolyte solution D (Figure 3c), distinct cracks are visible but the inset displays that the distribution and surface morphology are very similar to that of the pristine electrode. No visible surface layer has formed on the electrode during cycling in solution D. Nevertheless, the particles morphology has changed compared to that of the pristine electrode (Figure 3a), which is probably caused by the conversion reaction corresponding to equation (3), (4), and (7). If comparing the electrodes cycled in solution D (Figure 3c) and F (Figure 3d), the cracks appearing in solution D are larger, which also indicates missing elasticity of the surface layer.

To thoroughly understand the impact of the electrode's surface layers on their electrochemical behavior, we performed a surface analysis by using energy-dispersive spectroscopy and x-ray photoelectron spectroscopy. The corresponding results are presented in Figure 4 and Figure 5, respectively. An Sb signal can clearly be detected in the EDS maps for the pristine electrode (Figure 4a) as well as for electrodes cycled in solution D (Figure 4c) and F (Figure 4d). Different from that, the Sb signal is very weak in most areas of the electrode cycled in solution E (Figure 4b). The imaging depth of EDS is in a range of ~1 μm at 10 kV. Hence, the surface layer formed in solution E is relatively thick, exceeding the nanometer range. Such a thick surface layer could form in the presence of decomposition products and lead to a capacity decline throughout the cycling process. Different from that, surface reactions in solutions D and F provide surface layers, which are thinner than 1 μm. For this reason, XPS spectra were recorded in order to enable comparison among the surface films thicknesses of the respective cycled electrodes. The presence of an Sb^{3+} $3d_{5/2}$ signal in the Sb 3d spectra and a Sb_2O_3 signal in the O 1s spectra indicate that the surface layer is thinner than 10 nm as this is the imaging depth of XPS. These signals are solely present for the pristine electrode (Figure 5b) as well as for electrodes cycled in electrolyte solution D (Figure 5h). Sb signals are neither existing in spectra related to electrodes cycled in solution E (Figure 5d) nor spectra of electrodes cycled in solution F (Figure 5f). Consequently, the surface layers' thicknesses depending on the related electrolyte solution in which the electrodes were cycled are <1 μm for solution E, between 10 nm and 1 μm for solution F and >10 nm for solution D. The presence of FEC helps to form flexible surface layers with an adequate thickness, which can improve the electrochemical performance (Figure 2). In general, the surface layers on the electrodes cycled in all 3 solutions consist of the same carbon-containing species in different ratios indicated in the C 1s spectra (Figure 5a, c, e, g). These different amounts of the characterized surface species arise from different interactions of the solvents with Sb_2O_3, the conductive carbon and also the CMC-binder. However, understanding the specific influence of these species is beyond the scope of this work. A further evaluation of the electrodes' surface chemistry in solution E is not implemented in the following course of this study, as the influence of parasitic reactions and decomposition products reasonably explains the poor electrochemical performance and these issues were already discussed elsewhere.[10,16]

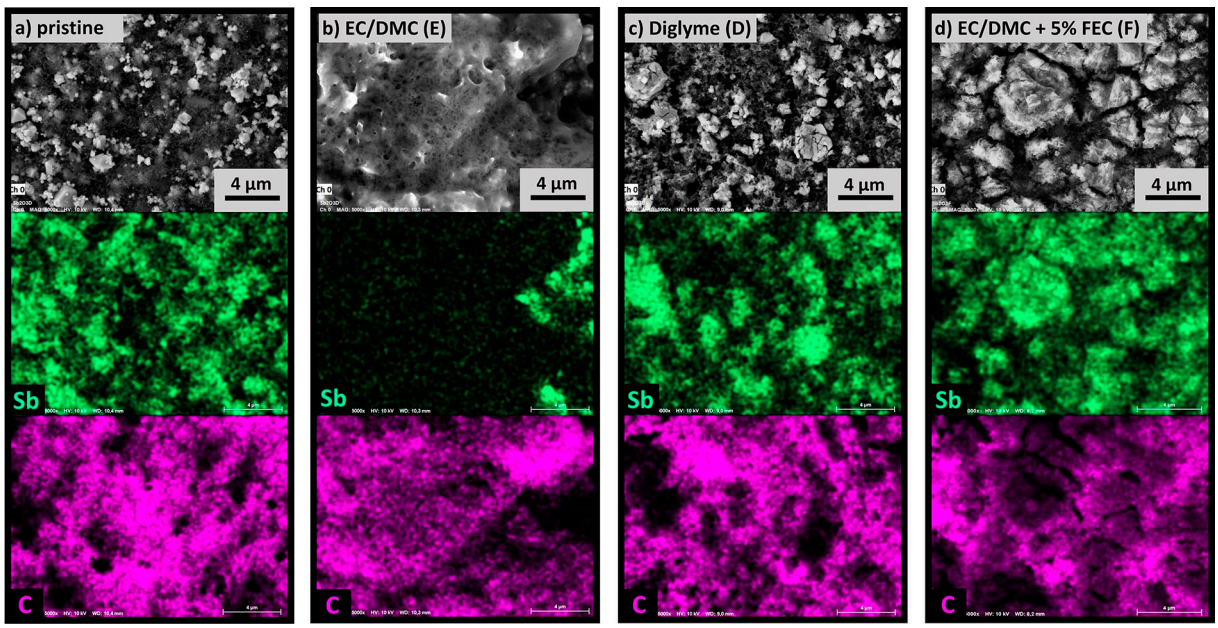

Figure 4. Scanning electron microscopy images and EDS maps of Sb_2O_3 electrodes: a) pristine, b) after 50 cycles in solution E, c) after 50 cycles in solution D, d) after 50 cycles in solution F. EDS signals of antimony are highlighted in green and signals of carbon in magenta.

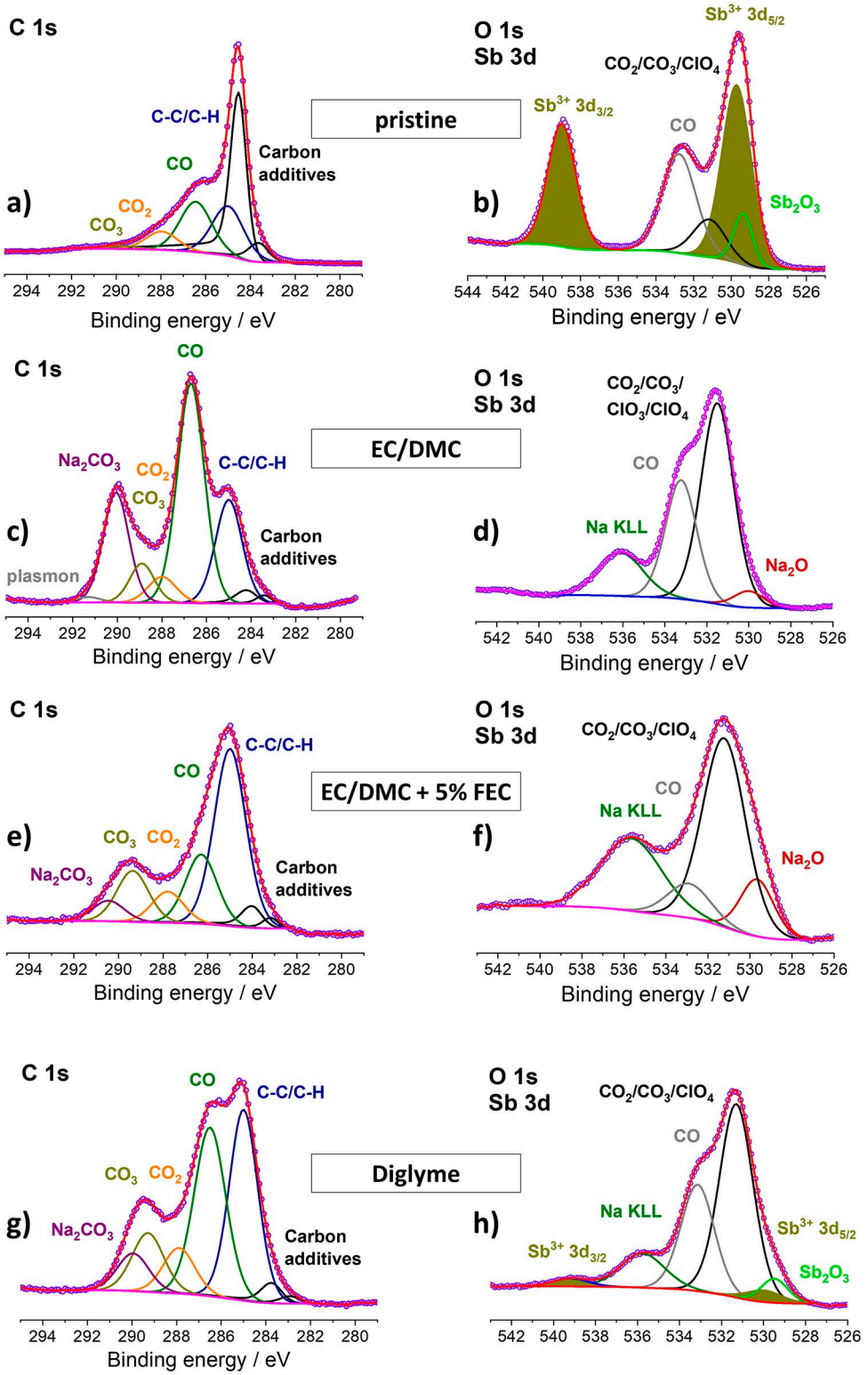

Figure 5. C 1s, O 1s and Sb 3d XPS spectra of Sb_2O_3 electrodes: a, b) pristine; c, d) after 50 cycles in solution E; e, f) after 50 cycles in solution F; g, h) after 50 cycles in solution D.

2.4. Ex Situ Characterization of the Electrolyte and Sodium-Metal Counter Electrode

An *ex-situ* optical analysis of the cycled electrolyte solutions (Figure 6a, b), separators (Figure 6c, d) and counter electrodes (Figure 6e, f) was conducted after cycling in solutions D and F, respectively. The postmortem analyses of the solutions, electrodes and separators after cell cycling in solutions D and F emphasizes well the difference between a suitable (F) and unsuitable (D) solution. Previous to the electrochemical cycling, the electrolyte solutions were both clear and colorless. The GF/D separators were plain white discs and the sodium counter electrodes were shiny metallic discs. Most obviously, a strong color change occurred with the solution (Figure 6a), the separator (Figure 6c) and the sodium counter electrode for cells cycled with solution D (Figure 6e). In contrast, a similar analysis of cells cycled with solution F does not show any pronounced changes. The electrolyte solutions presented in Figure 6a-b were analyzed by inductively coupled plasma mass spectrometry to determine the Sb content. Both pristine electrolyte solutions contained $< 0.022\ mg\,L^{-1}$ Sb. After 50 cycles, $12.3\ mg\,L^{-1}$ Sb were detected in solution D and $0.5\ mg\,L^{-1}$ Sb was detected in solution F. Consequently, the Sb quantity in cycled solution D is ~24 times higher than in cycled solution F.

In order to further examine the behavior of the dissolved Sb species on the counter electrodes, we analyzed the cycled sodium metal counter electrodes by SEM and EDS (Figure 7). The surfaces of the Na counter electrodes cycled in cells containing solution F have smooth textures and do not show any visible surface films in the SEM images (Figure 7a). In contrast, the surfaces of the Na counter electrodes cycled in cells containing solution D are covered by a porous film (Figure 7b). Additionally, a ~10 µm sized round shaped particle was found embedded in the surface film of the Na electrode cycled in solution D. The associated EDS map is shown in Figure 7c-d. No antimony is found on the counter electrode cycled in cells with solution F (Figure 7c). In contrast, the large round-shaped particles visible on the Na electrodes from cells cycled with solution D can be identified as Sb containing materials (Figure 7d). Moreover, antimony signals were solely present on the surfaces of Na counter electrodes cycled in cells that contained electrolyte solution D (Figure 7e).

2.5. Proposed Mechanism that Explains the Behavior of Sb_2O_3 Electrodes Cycled in Diglyme-Based Electrolyte Solutions

Based on the results provided throughout this study, we expect that the ether coordinates and dissolves Sb^{3+}, which is formed during de-sodiation. This hypothesis is supported by the work of Koshima and Onishi.[30] These authors describe the extraction

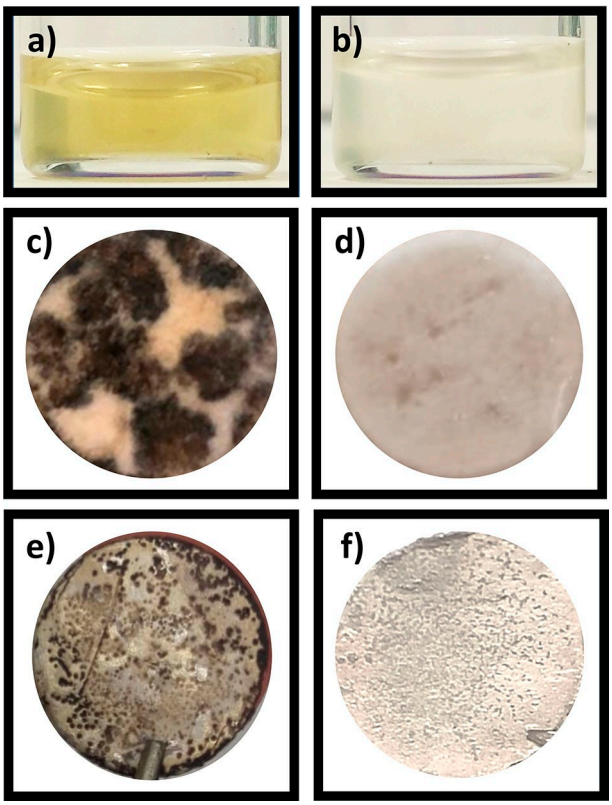

Figure 6. Cell components removed after 50 cycles: a) electrolyte solution D, b) electrolyte solution F, c) separator cycled in solution D, d) separator cycled in solution F, e) sodium-metal counter electrode cycled in solution D, f) sodium-metal counter electrode cycled in solution F.

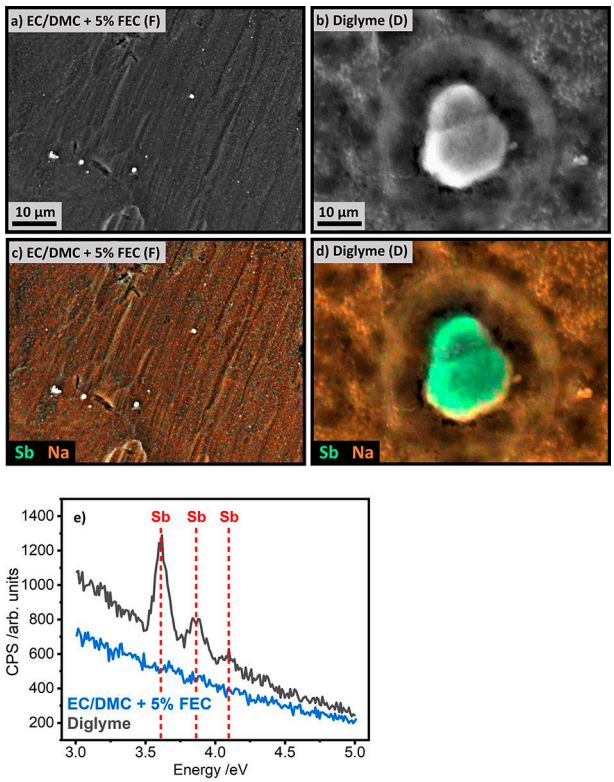

Figure 7. Scanning electron microscopy images and the corresponding EDS maps of the sodium counter electrode after 50 cycles in a,c) electrolyte solution F, b,d) electrolyte solution D. EDS signals of antimony are highlighted in green and signals of sodium are highlighted in orange.e) Comparison of EDS spectra of the sodium counter electrodes cycled in electrolyte solutions F and D, respectively (Sb signals are marked in red).

of Sb^{3+} with crown ethers. It was possible to extract 96–94% Sb^{3+} from a hydrochloric acid solution due to the coordination features of the ethers. Furthermore, Beagley *et al.*[31] also described ether-based complexes of Sb^{3+}. If Sb^{3+} cations are dissolved in the electrolyte solution due to the ability of diglyme to coordinate to the Sb ions, they can migrate to the sodium metal counter electrodes and be reduced therein to metallic antimony. Subsequently, metallic Sb is plated on the sodium metal due to the low redox potential of Na (Figure 7d). These additional side processes interfere with the processes presented in equations (1)-(7) above. Such scenarios induce extremely non-uniform reactions in sodium-ion battery systems, as we observed with cells containing diglyme based solutions (denoted as D) (Figure 2d). Of course, an easy dissolution of Sb cations is facilitated by the absence of passivating surface films on the electrodes in diglyme solutions, because of the relatively low intrinsic reactivity of ether solvents (in general) towards active metals such as Li and Na.[20,32] The de-sodiation is accompanied by constant dissolution of the active material and its simultaneous deposition on the counter electrode. Such additional mechanisms most probably cause an irregular de-sodiation profile and an unexpectedly high de-sodiation capacity. Side processes like a dissolution of the active material can badly affect any formation of protective surface films. The obvious result of this problematic situation is the poor cycling stability of cells containing the ethereal electrolyte solution denoted as D (Figure 2a) and the strange cycling efficiency (Figure 2b). In summary, the high content of Sb in the cycled diglyme-based electrolyte solution and on the Na counter electrodes taken from cycled cells, proves that the active material is indeed dissolved in in these cells. We also found minor amounts of Sb in cycled FEC containing solutions (denoted as F). However, the Sb quantity in cycled glyme based solutions was ~24 times higher than the trace Sb content found in cycled FEC containing solutions. The yellow shade of the cycled solution D (Figure 6a) further reflects the presence of dissolved Sb ions inside this electrolyte solution.

3. Conclusions

This study provides important findings concerning the influence of electrolyte solutions on the behavior of Sb_2O_3 based anodes for sodium-ion-batteries. Significant emphasis was put on the impact of the nature of the solvents in the electrolyte solutions. Here, the impact of important solvents like EC/DMC, EC/DMC + 5% FEC and Diglyme for sodium-ion batteries were compared. We first highlight the positive effect of FEC when served as an additive in EC/DMC solvent-based electrolyte solutions. In contrast to the case of an additive-free electrolyte solution, the presence of FEC in EC/DMC based electrolytes leads to the formation of thin, compact and probably elastic surface films that passivate the Sb_2O_3 electrodes and avoid their morphological disintegration (e.g., cracking phenomena). The presence of this valuable additive also helps to protect the sodium counter electrodes from detrimental side reactions with the electrolyte solution. This leads to >80% capacity retention of Sb_2O_3 electrodes after 100 cycles in cells containing Na metal counter electrodes. Unlike that, in additive-free electrolyte solutions, the electrodes' capacity is fully lost after 70 cycles. In parallel, a thick, non-uniform surface layer is formed. This surface layer is composed of degradation products originating from surface reactions of the Na metal electrodes with the electrolyte solution. These reactions can occur intensively in the absence of sufficient passivation.

Considering the diglyme based solutions, we highlight their ability to dissolve Sb based active materials during electrochemical cycling. Upon the oxidation of Sb to Sb^{3+} in the course of the conversion reaction (de-sodiation, discharging), the ether solvent most probably coordinates and dissolves Sb^{3+} cations. Also, due to the relatively low reactivity of diglyme towards Na metal electrodes (and reducing Na compounds), protective surface layers cannot be formed in sodium-containing cells with diglyme based electrolyte solutions. Thereby, possible dissolution of Sb ions cannot be avoided in these systems. Moreover, we suggest that possible complexation of Sb cations by diglyme molecules promotes their dissolution and migration to the Na metal counter electrode side. This has a detrimental effect on the cell performance, as the dissolved Sb species are deposited on the sodium counter electrode. The use of such a solvent with high complexation affinity may be problematic for all kinds of electrodes based on conversion reactions, which contain transition-metal elements. This explains the detrimental effects of glymes on NIBs that were described in other studies.[17,20] Interestingly, the negative impact of diglyme on conversion anodes comprising antimony oxide, as reported herein, was not observed with conversion anodes comprising tin compounds.[18,21] Hence, the unique interactions between Sn cations and diglyme molecules do not exist when we change the central transition metal involved in the electrode's conversion reactions. This situation emphasizes the importance of a proper adjustment of specific characteristics, upon selecting electrolyte solutions for the individual sodium-ion battery system.

Experimental Section

Electrolyte Solutions

The preparation and handling of the solvents and salts were conducted in an argon-filled glovebox (MBraun, O_2, H_2O < 0.5 ppm). The sodium salt was dried under vacuum at 80 °C for 48 h. Three different organic electrolytes solutions were prepared: 1 M sodium perchlorate ($NaClO_4$, Alfa Aesar, >99% purity) was dissolved in a mixture of 1:1 (by mass) ethylene carbonate (EC, Sigma Aldrich, ≥99% purity) and dimethyl carbonate (DMC, Sigma Aldrich, ≥99% purity), respectively. As an additional electrolyte solution, 5 mass% fluoroethylene carbonate (FEC, Sigma Aldrich, 99% purity) was added to the previous mixture. As third electrolyte solution, a 1 M solution of $NaClO_4$ in bis(2-methoxyethyl) ether (Diglyme, Sigma Aldrich, anhydrous, 99.5% purity) was applied. All prepared electrolyte solutions were examined via Karl-Fischer titration and were found to contain less than 25 ppm water. The electrolytes will be referred to as D (1 M $NaClO_4$ in diglyme), E (1 M $NaClO_4$ in EC/DMC) and F (1 M $NaClO_4$ in EC/DMC + 5% FEC).

Electrolyte Solution Characterization

For visual analysis of the electrolyte solutions reactivity, the electrolyte solution was removed from the cycled cells with a syringe in the argon-filled glove box. Pictures of the electrolyte solutions were recorded immediately after transferring the liquid into glass vessels. The cells were further disassembled, and additional pictures of the separator and sodium metal counter electrode were taken while keeping the electrodes inside the glovebox. The Sb content from the extracted electrolyte was determined by inductively coupled plasma mass spectrometry (ICP-MS).

Electrode Materials and Preparation

Sb_2O_3-based working electrodes were prepared by mixing Sb_2O_3 (Sigma Aldrich, nanopowder, <250 nm particle size (TEM), $\geq 99.9\%$ trace metals basis) with C-NERGY C65 conductive carbon additive (Imerys Graphite & Carbon) and a CMC solution in a DAC150.1 FVZ speed-mixer from Hauschild. The dry electrode composition was 70 mass% Sb_2O_3, 20 mass% C65, and 10 mass% CMC.

The active material powder and conductive additive were first dry-mixed at 1000 rpm for 5 min. Then, a water/ethanol solution was added to obtain a viscous paste. This paste was again mixed at 1500 rpm for 10 min following 2500 rpm for 10 min. After 10 min of sonication, the paste was again mixed at 2500 rpm for 10 min before adding the binder solution (3 mass% CMC in water). The last mixing step was conducted at 800 rpm for 10 min. The slurries were doctor bladed on an aluminum foil and dried for three days at ambient conditions. Subsequently, the electrodes were punched out with a 12 mm diameter and transferred into a vacuum oven inside an Ar-filled glovebox. Finally, a vacuum drying step at 120 °C for 12 h was conducted. The thickness of the dried electrodes was typically 30–40 μm with a mass loading of 3 ± 1 mg cm^{-2} (the full electrode mass, including the current collector, was 7 ± 1 mg cm^{-2}).

Cell Preparation and Electrochemical Characterization

Custom-built polyether ether ketone (PEEK) cells with spring-loaded titanium pistons as three-electrodes systems were used for electrochemical testing as described in Ref.[33]. After drying all the cells parts at 120 °C, the cells were assembled inside an Ar-filled glovebox. When using sodium metal as a counter and a reference electrode, great importance was paid to the preparation as proposed in Ref.[34]. The oxide layer was removed thoroughly with a particular care to obtain a smooth Na metal surface and to avoid inhomogeneity and impurities. The counter electrodes were pressed to a uniform thickness of 1 mm. 12 mm diameter sodium disc counter electrodes and the working electrodes were separated by a 13 mm diameter vacuum dried glass-fiber disc (Whatman GF/D). Cells that were cycled for XPS and SEM analyses were additionally separated by a cellulose separator (Nippon Kodoshi). This separator was placed on the top of the working electrode or the respective sodium disc to avoid the adhesion of glass fibers on the surface. A copper foil current collector was placed on the backside of each counter electrode. The Na-reference electrode was placed on a compressed glass fiber separator (GF/D, from Whatman) in a cavity close to the working electrode/counter electrode stack and contacted by a titanium wire. The cells were vacuum filled with the respective electrolyte.

Electrochemical measurements were carried out in a climate chamber at 25 °C using a VMP3 multi-channel potentiostat/galvanostat (Bio-logic Science Instrument), equipped with the EC-Lab software. Galvanostatic charge/discharge cycling with potential limitation (GCPL) experiments was performed in a voltage window of 0.1–2.0 V vs. Na/Na^+ with a charge/discharge current of 200 mA g^{-1}. All capacity values stated in this work are given with respect to the active electrode mass (Sb_2O_3 mass). The cycling stability measurements were stopped after 100 cycles. Cells that were prepared for XPS and SEM analysis were stopped after 50 cycles in the de-sodiated state.

Electrodes and Materials Characterization

X-ray diffraction (XRD) measurements of the Sb_2O_3 powder were performed with an STOE STADI P diffractometer (Mo–Kα-radiation, $\lambda = 0.7093$ Å) in rotating capillary transmission mode. For phase identification, the ICSD database was utilized.

Scanning electron microscopy (SEM) and energy dispersive X-ray spectroscopy (EDS) measurements were conducted by a thermal field emission scanning electron microscope (FESEM, Carl Zeiss SMT AG) equipped with energy-dispersive spectroscopy (EDS, Quantax 400 SDD, Bruker) at an acceleration voltage of 7 kV. The samples were fixed on a steel sample holder by using sticky tape. The Sb_2O_3 powder sample was sputtered with a 5 nm thick gold/palladium layer.

For the ex-situ XPS and SEM/EDS analyses, the electrodes were charged-discharged 50 times and stopped in the de-sodiated state at 2.0 V vs. Na/Na^+. The potential was held for 2 h. The cells were then transferred to an Ar-filled glovebox for disassembly. The working electrodes were removed and rinsed with DMC or Diglyme prior to XPS and SEM/EDS measurements. The sodium metal counter electrode was characterized without subsequent rinsing to avoid the removal of soluble Sb-containing species. The samples were constantly kept in inert gas atmosphere also while transferring.

X-ray photoemission measurements were performed using a K-Alpha XPS spectrometer from Thermo Fisher Scientific (East Grinstead). The samples were illuminated with monochromatic Al–Kα X-rays with a spot size of about 400 μm. The photoelectrons were detected with a hemispherical 180 dual focus analyzer with 128 channel detectors. To prevent any localized charge buildup, the K-Alpha charge compensation system was employed during analysis, using electrons of 8 eV energy and low-energy argon ions. The Thermo Avantage software was used for data acquisition and processing.[35] The spectra were fitted with one or more Voigt profiles (binding energy uncertainty: ±0.2 eV). All spectra were referenced to the C 1s peak of hydrocarbon at 285.0 eV binding energy controlled by means of the well-known photoelectron peaks of metallic Cu, Ag, and Au.

Acknowledgements

The authors thank Dr. A. Sarapulova, Dr. M. Widmaier, M. Bauer, and C. Li for support and helpful discussions. This work contributes to the research performed at CELEST (Center for Electrochemical Energy Storage Ulm-Karlsruhe) and was funded by the German Research Foundation (DFG) under Project ID 390874152 (POLiS Cluster of Excellence). We further thank Thomas Bergfeldt and the IAM-AWP, Chemical Analytics Institute for conducting the ICP-MS analytics. Open access funding enabled and organized by Projekt DEAL.

Conflict of Interest

The authors declare no conflict of interest.

Keywords: non-aqueous electrolyte solutions · conversion reactions · Sb ions complexation · sodium batteries · diglyme

[1] D. Kundu, E. Talaie, V. Duffort, L. F. Nazar, *Angew. Chem.* **2015**, *54*, 3431–3448.
[2] J.-M. Tarascon, *Nat. Chem.* **2010**, *2*, 510.
[3] V. Palomares, P. Serras, I. Villaluenga, K. B. Hueso, J. Carretero-González, T. Rojo, *Energy Environ. Sci.* **2012**, *5*, 5884.
[4] A. Ponrouch, E. Marchante, M. Courty, J.-M. Tarascon, M. R. Palacín, *Energy Environ. Sci.* **2012**, *5*, 8572.
[5] J. Barker, M. Y. Saidi, J. L. Swoyer, *Electrochem. Solid-State Lett.* **2003**, A1-A4.
[6] P. Senguttuvan, G. Rousse, V. Seznec, J.-M. Tarascon, M. R. Palacín, *Chem. Mater.* **2011**, *23*, 4109–4111.
[7] a) M. Dahbi, N. Yabuuchi, K. Kubota, K. Tokiwa, S. Komaba, *Physical Chemistry Chemical Physics: PCCP* **2014**, *16*, 15007–15028; b) N. Yabuuchi, K. Kubota, M. Dahbi, S. Komaba, *Chem. Rev.* **2014**, *114*, 11636–11682.
[8] M. D. Slater, D. Kim, E. Lee, C. S. Johnson, *Adv. Funct. Mater.* **2013**, *23*, 947–958.
[9] Y. Sun et al., *Nat. Commun.* **2013**, *4*, 1870.
[10] K. Pfeifer, S. Arnold, J. Becherer, C. Das, J. Maibach, H. Ehrenberg, S. Dsoke, *ChemSusChem* **2019**, *12*, 3312–3319.
[11] B. L. Ellis, L. F. Nazar, *Curr. Opin. Solid State Mater. Sci.* **2012**, *16*, 168–177.
[12] F. Klein, B. Jache, A. Bhide, P. Adelhelm, *Physical Chemistry Chemical Physics: PCCP* **2013**, *15*, 15876–15887.
[13] M. R. Palacín, *Chem. Soc. Rev.* **2009**, *38*, 2565–2575.
[14] C. Li, A. Sarapulova, K. Pfeifer, S. Dsoke, *ChemSusChem* **2020**.
[15] a) D. Su, H.-J. Ahn, G. Wang, *Chem. Commun.* **2013**, *49*, 3131–3133; b) R. Malini, U. Uma, T. Sheela, M. Ganesan, N. G. Renganathan, *Ionics* **2009**, *15*, 301–307.
[16] K. Pfeifer, S. Arnold, Ö. Budak, X. Luo, V. Presser, H. Ehrenberg, S. Dsoke, *J. Mater. Chem. A* **2020**, *8*, 6092–6104.
[17] M. Hu, Y. Jiang, W. Sun, H. Wang, C. Jin, M. Yan, *ACS Appl. Mater. Interfaces* **2014**, *6*, 19449–19455.
[18] K. Li et al., *Nat. Commun.* **2019**, *10*, 725.
[19] X. Liu, B. Qin, H. Zhang, A. Moretti, S. Passerini, *ACS Appl. Energy Mater.* **2019**, *2*, 2786–2793.
[20] K. Westman et al., *ACS Appl. Energy Mater.* **2018**, *1*, 2671–2680.
[21] W. Brehm, J. R. Buchheim, P. Adelhelm, *Energy Technol.* **2019**, *7*, 1900389.
[22] a) C. Cui et al., *Nano Lett.* **2019**, *19*, 538–544; b) Y. Zhu, X. Han, Y. Xu, Y. Liu, S. Zheng, K. Xu, L. Hu, C. Wang, *ACS Nano* **2013**, *7*, 6378–6386.
[23] A. Darwiche, C. Marino, M. T. Sougrati, B. Fraisse, L. Stievano, L. Monconduit, *J. Am. Chem. Soc.* **2012**, *134*, 20805–20811.
[24] J. Qian, Y. Chen, L. Wu, Y. Cao, X. Ai, H. Yang, *Chem. Commun.* **2012**, *48*, 7070–7072.
[25] H. Lu, L. Wu, L. Xiao, X. Ai, H. Yang, Y. Cao, *Electrochim. Acta* **2016**, *190*, 402–408.
[26] R. Dugas, A. Ponrouch, G. Gachot, R. David, M. R. Palacin, J. M. Tarascon, *J. Electrochem. Soc.* **2016**, A2333–A3339.
[27] S. S. Zhang, *J. Power Sources* **2006**, *162*, 1379–1394.
[28] A. Darwiche, L. Bodenes, L. Madec, L. Monconduit, H. Martinez, *Electrochim. Acta* **2016**, *207*, 284–292.
[29] L. Bodenes, A. Darwiche, L. Monconduit, H. Martinez, *J. Power Sources* **2015**, *273*, 14–24.
[30] Hideko Koshima, Hiroshi Onishi, *Analyst* **1986**, 1261–1264.
[31] Brian Beagley, Monica Endregard, David G. Nicholson, *Acta Chem. Scand.* **1991**, 349–353.
[32] M. Han, C. Zhu, T. Ma, Z. Pan, Z. Tao, J. Chen, *Chem. Commun.* **2018**, *54*, 2381–2384.
[33] D. Weingarth, M. Zeiger, N. Jäckel, M. Aslan, G. Feng, V. Presser, *Adv. Energy Mater.* **2014**, *4*, 1400316.
[34] J. Conder, C. Villevieille, *Chem. Commun.* **2019**, *55*, 1275–1278.
[35] K. L. Parry, A. G. Shard, R. D. Short, R. G. White, J. D. Whittle, A. Wright, *Surf. Interface Anal.* **2006**, *38*, 1497–1504.

Manuscript received: July 3, 2020
Revised manuscript received: July 16, 2020
Accepted manuscript online: July 21, 2020